Functionalized Carbon Nanotubes with Tethered Pyrenes: Synthesis and Photophysical Properties

Robert B. Martin,[†] Liangwei Qu,[†] Yi Lin,[†] Barbara A. Harruff,[†] Christopher E. Bunker,[‡] James R. Gord,[‡] Lawrence F. Allard,[§] and Ya-Ping Sun*[,†]

Department of Chemistry, Howard L. Hunter Chemistry Laboratory, Clemson University, Clemson, South Carolina 29634-0973, Air Force Research Laboratory, Propulsion Directorate, WPAFB, Ohio 45433-7103, and High-Temperature Materials Laboratory, Oak Ridge National Laboratory, Oak Ridge, Tennessee 37831-6062

Received: March 5, 2004; In Final Form: May 24, 2004

Single-walled (SWNTs) and multiple-walled carbon nanotubes (MWNTs) were functionalized with dendra of tethered pyrene species, where the tether length was varied. These functionalized carbon nanotube samples are soluble in common organic solvents, making it possible to characterize the samples and to investigate and compare the photophysical properties of the tethered pyrene moieties in homogeneous solution. In general, the pyrene monomer excited state is significantly quenched by two competing processes of "intramolecular" excimer formation and energy transfer to the nanotube. The excimer formation is dynamic in nature, and the excimer emission is also quenched by the energy transfer, contributing to the overall low fluorescence quantum yields and rapid fluorescence decays. There are effects of the tether length on photoexcited-state properties of the pyrene species according to a comparison of the results obtained in solution vs in solid-state polymer matrix. The structurally more flexible environment for the pyrene moiety associated with a longer tether is more favorable to the excimer formation and less favorable to the excited-state energy transfer. The mechanistic implication of the results and potential applications of such materials are discussed.

Introduction

Carbon nanotubes have attracted much recent attention for a variety of potential technological applications, including those in electronic and optoelectronic devices and chemical and biochemical sensors.[1−5] It is generally acknowledged that chemical modification of carbon nanotubes with specific functionalities is required for many of these potential applications. In particular, the functionalization of carbon nanotubes with well-characterized chromophores represents an emerging strategy in the development of nanoscale photoactive materials.[6−10] Equally important is the fact that the solubilization as a result of the modification or functionalization makes it possible to study the properties of carbon nanotubes in homogeneous solution.

There have been some recent reports on attaching chromophore molecules to both single-walled (SWNT) and multiple-walled (MWNT) carbon nanotubes and on photophysically investigating the excited-state properties of the resulting materials and the effects of chromophore-nanotube interactions. For example, it was reported that derivatized pyrenes[11,12] and porphyrins[10,13] could be attached to carbon nanotubes noncovalently and that the chromophores on the nanotube surface became less fluorescent.[12,13] However, according to Zhang et al., when anthracene molecules were chemisorbed on the SWNT surface, there was no significant quenching of anthracene photoexcited state by the nanotube.[14] Instead, the anthracene emission maximum red-shifted, which was interpreted as an indication for intermolecular electron transfer.[14]

The chromophores covalently attached to carbon nanotubes generally have different photophysical properties from those of the noncovalently attached ones.[7,8,15,16] The stability in the chromophore − nanotube relationship provided by the covalent linkage makes it less ambiguous in the probing of interactions between photoexcited chromophore species and the nanotube. According to Georgakilas et al., upon the 1,3-dipolar addition of pyrene-containing azomethine ylides to the nanotube sidewall, the fluorescence of the pyrene moieties became short-lived with low quantum yield.[15] Sun and co-workers functionalized SWNTs with pyrene-containing dendra via the esterification of the nanotube-bound carboxylic acids.[16] It was found that the nanotube-tethered pyrene moieties form excimers and that both pyrene monomer and excimer emissions are quenched effectively by the tethered nanotube via efficient "intramolecular" energy transfers.[16]

We have extended our investigation on the functionalization of carbon nanotubes with pyrene-containing dendra to examine the difference between SWNTs and MWNTs and to evaluate effects of the tether length. Here we report on the synthesis and characterization of the functionalized carbon nanotubes and a systematic photophysical study of the excited-state pyrene − nanotube interactions. The results show that there are significant emission contributions from pyrene excimers in all of these functionalized carbon nanotube samples in solution and that both SWNTs and MWNTs serve as efficient quenchers for the pyrene photoexcited states. The photophysical properties of the pyrene moieties in the different functionalized carbon nanotube samples are compared and discussed.

* Corresponding author. E-mail: syaping@clemson.edu.
[†] Clemson University.
[‡] Air Force Research Laboratory, Propulsion Directorate, WPAFB.
[§] Oak Ridge National Laboratory.

10.1021/jp048984s CCC: $27.50
Published on Web 07/09/2004

SCHEME 1

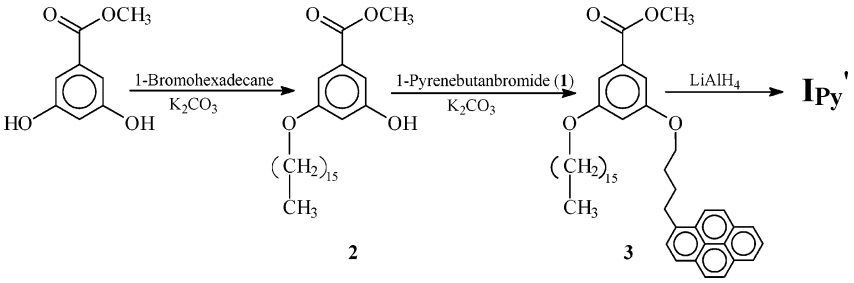

Experimental Section

Materials. Methyl 3,5-dihydroxybenzoate (98%) and 18-crown-6 (98%) were purchased from Avocado Research Chemical Ltd., thionyl chloride (99.5%), potassium carbonate (anhydrous), and 1-bromohexadecane (99%) from Acros, 1-pyrenemethanol, 1-pyrenebutanol (98%), and phosphorus tribromide from Aldrich, and magnesium sulfate (99.5%) and lithium tetrahydridoaluminate (95%) from Alfa Aesar. THF was distilled over sodium before use. Diethyl ether and other solvents were either of spectrophotometry/HPLC grade or purified via simple distillation. Poly(methyl methacrylate) (PMMA, average molecular weight ~ 350,000) was obtained from Acros. Deuterated NMR solvents were supplied by Cambridge Isotope Laboratories.

Samples of SWNTs and MWNTs produced via the arc-discharge[17] and chemical vapor deposition[18] methods, respectively, were supplied by Prof. A. M. Rao (Department of Physics and Astronomy, Clemson University). Both samples were purified via the oxidative acid treatment well-established in the literature.[19] Briefly, a nanotube sample (1 g) was suspended in an aqueous HNO_3 solution (2.6 M, 1.5 L) and refluxed for 48 h. Upon vigorous centrifuging, the supernatant was discarded, and the remaining solids were washed repeatedly with deionized water until neutral pH and then dried under vacuum.

1-Pyrenebutanbromide (1). To a solution of 1-pyrenebutanol (0.70 g, 2.55 mmol) in toluene (50 mL) was added phosphorus tribromide (0.76 g, 2.8 mmol), followed by refluxing for 4 h. The reaction mixture was washed with water several times, dried with anhydrous $MgSO_4$, and evaporated to remove the solvent toluene to obtain **1** (98% yield).[20]

Methyl 3-Hydroxy-5-hexadecoxy Benzoate (2). A solution of methyl 3,5-dihydroxybenzoate (2 g, 11.9 mmol), potassium carbonate (8.1 g, 58.6 mmol), and 18-crown-6 (0.25 g, 0.94 mmol) in solvent mixture of THF (150 mL) and acetonitrile (30 mL) was prepared, and to the solution was added 1-bromohexadecane (1.83 g, 6 mmol). After the mixture was refluxed for 10 h, the solvent was removed on a rotary evaporator. The sample was redissolved in chloroform, and the chloroform solution was washed with water several times and dried with anhydrous $MgSO_4$. The crude product was purified on a silica gel column with chloroform as eluting solvent to obtain **2** (43% yield).[20]

Methyl 3-Hexadecoxy-5-pyrenebutanoxyl Benzonate (3). A solution of **1** (0.227 g, 0.676 mmol), **2** (0.265 g, 0.676 mmol), potassium carbonate (0.21 g, 1.5 mmol), and 18-crown-6 (0.1 g, 0.37 mmol) in solvent mixture of THF (10 mL) and acetonitrile (50 mL) was refluxed for 20 h. After the solvent removal on a rotary evaporator, the solid sample was redissolved in chloroform. The chloroform solution was washed with water several times and dried with anhydrous $MgSO_4$. The crude product was purified on a silica gel column with chloroform as eluting solvent to obtain **3** (98% yield) (see Scheme 1).[20]

I_{Py} and I_{Py}'. The synthesis of I_{Py} (3-decyloxy-5-pyrenyloxyphenylmethan-1-ol) has been reported elsewhere.[16] For I_{Py}' (3-decyloxy-5-pyrenyloxyphenylbutan-1-ol), to a solution of **3** (1.6 g, 2.6 mmol) in dry diethyl ether (25 mL) was added lithium tetrahydridoaluminate (0.12 g, 3.1 mmol). After the solution was refluxed for 8 h, water (2 mL) was added to quench the reaction. The reaction mixture was filtered to yield the crude product, followed by purification on a silica gel column with chloroform as eluting solvent to obtain I_{Py}' (95% yield). ^{1}H NMR (500 MHz, $CDCl_3$): δ 0.88 (t, J = 7.1 Hz, 3H), 1.10−1.37 (m, 24H), 1.42 (m, 2H), 1.75 (m, 2H), 1.95 (m, 2H), 2.05 (m, 2H), 3.42 (t, J = 7.8 Hz, 2H), 3.91 (t, J = 6.4 Hz, 2H), 4.00 (t, J = 6.3 Hz, 2H), 4.60 (s, 2H), 6.37 (t, J = 2.05 Hz, 1H), 6.48 (d, J = 1.80 Hz, 2H), 7.88 (d, J = 8.2 Hz, 1H), 7.96−8.05 (m, 3H), 8.08−8.13 (m, 2H), 8.13−8.19 (m, 2H), 8.28 (d, J = 9.65 Hz, 1H) ppm; ^{13}C NMR (125 MHz, $CDCl_3$): δ 14.23, 22.79, 26.14, 28.32, 29.30, 29.34, 29.46, 29.49, 29.68, 29.70, 29.76, 29.79, 32.02, 33.25, 65.53, 67.83, 68.15, 100.64, 105.09, 105.21, 123.49, 124.77, 124.88, 124.94, 125.11, 125.18, 125.89, 126.68, 127.33, 127.36, 127.60, 128.72, 129.94, 130.98, 131.51, 136.63, 143.28, 160.50, 160.62 ppm. (See Scheme 2.)

Nanotube Functionalization. The functionalization of carbon nanotubes with I_{Py} or I_{Py}' was accomplished via the esterification of the nanotube-bound carboxylic acids.[21] The detail on the synthesis of **I_{Py}-SWNT** has been reported elsewhere.[16] Similarly, in the preparation of **I_{Py}**-MWNT, a purified MWNT sample (27 mg) was refluxed with $SOCl_2$ (5 mL) for 24 h to convert the nanotube-bound carboxylic acids into acyl chlorides. After a complete removal of unreacted $SOCl_2$ under vacuum, I_{Py} (150 mg, 0.26 mmol) was added to the acylated MWNT sample. The mixture was heated to 90 °C and vigorously stirred for 24 h under nitrogen protection. After being cooled to room temperature, the reaction mixture was extracted repeatedly with chloroform to obtain a dark-colored homogeneous solution. The solvent chloroform was evaporated, and the solid sample was purified in Soxhlet extraction with acetone for 24 h to remove primarily unreacted I_{Py}. Upon drying under vacuum at 60 °C for 24 h, **I_{Py}**-MWNT was obtained as a dark-colored solid. ^{1}H NMR (500 MHz, $CDCl_3$): 0.1−1.6 (broad), 1.6−2.2 (broad), 2.47 (broad), 2.76 (broad), 2.96 (broad), 3.1−5.2 (broad), 5.6−5.8 (broad), 5.9−6.7 (broad), 7.0−8.9 (broad) ppm. ^{13}C NMR (125 MHz, $CDCl_3$): 14.2, 22.8, 26.1, 29.5, 29.8, 32.0, 68.2, 124.9, 127.6, 129.1, 130.7 ppm.

I_{Py}'-SWNT was similarly prepared. In a typical experiment, a purified SWNT sample (20 mg) was treated in concentrated HCl solution to fully recover the carboxylic acid groups on the nanotube surface, followed by refluxing the sample in $SOCl_2$ (5 mL) for 24 h. After a complete removal of residual $SOCl_2$, the nanotube sample was mixed well with carefully dried I_{Py}' (200 mg, 0.32 mmol) in a flask. The mixture was heated to 100 °C and vigorously stirred for 24 h under nitrogen protection. After being cooled to room temperature, the reaction mixture

SCHEME 2

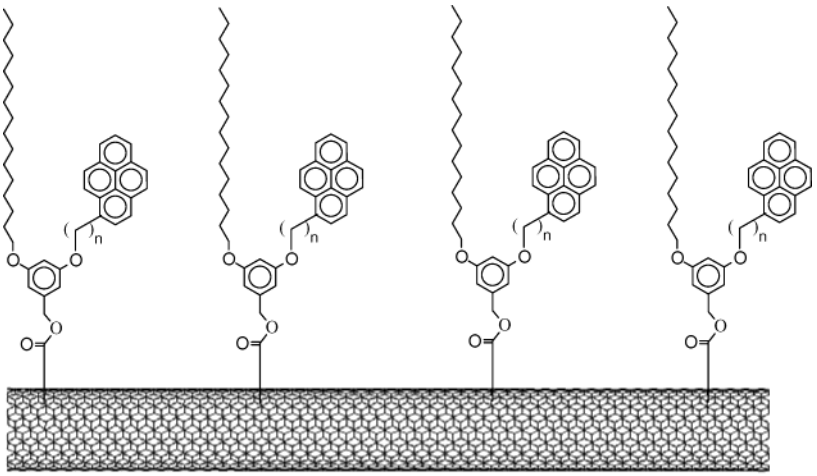

n = 1 $\mathbf{I_{Py}}$-SWNT
4 $\mathbf{I_{Py}}$'-SWNT

was extracted repeatedly with chloroform to obtain a dark-colored homogeneous solution. The solution was placed in a dialysis tubing (cutoff molecular weight ~1,000,000) in chloroform for 3 days to remove primarily unreacted $\mathbf{I_{Py}}'$. $\mathbf{I_{Py}}'$-SWNT was obtained as a dark-colored solid. ^{1}H NMR (500 MHz, $CDCl_3$): δ 0.1−2.4(broad), 2.5−5.1 (broad), 5.6−6.7 (broad), 7.4−8.5 (broad) ppm; ^{13}C NMR (125 MHz, $CDCl_3$): δ 14.2, 21.3, 22.8, 26.1, 28.2, 29.5, 29.8, 30.4, 32.0, 33.2, 34.3, 68.1 (broad), 96.2, 107.0, 107.7, 123.4, 124.8, 125.6, 125.8, 126.6, 127.2, 127.5, 128.3, 128.5, 129.7, 130.9, 131.4, 135.9, 136.6, 160.5 ppm.

Measurements. NMR spectra were obtained on a JEOL Eclipse +500 NMR spectrometer. Raman spectra were recorded on a Renishaw Raman spectrometer equipped with a 785 nm solid-state laser (50 mW). FT-IR spectra were measured on a Thermo-Nicolet Nexus 670 FT-IR spectrometer. Transmission electron microscopy (TEM) images were obtained on a Hitachi HF-2000 TEM system equipped with a Gatan Multiscan CCD camera for digital imaging. Thermogravimetric analysis (TGA) was carried out on a Mettler-Toledo TGA/SDTA851 system.

UV/vis absorption spectra were recorded on Shimadzu UV2101-PC and Perkin-Elmer Lambda 900 spectrophotometers. Emission spectra were measured on Spex Fluorolog-2 and Fluorolog-3 photon-counting emission spectrometers, both of which are equipped with a 450-W xenon source and a detector consisting of a Hamamatsu R928P PMT operated at −950 V. The Fluorolog-3 is also equipped with double monochromators for excitation and emission. Unless specified otherwise, all emission spectra were corrected for nonlinear instrumental response by use of predetermined correction factors.

Fluorescence decays were measured by using the time-correlated single-photon counting (TCSPC) method. The TCSPC setup consists of a nitrogen flash lamp (Edinburgh Instruments). The 337 nm light was isolated using a band-pass filter (10 nm fwhm). Fluorescence decays were monitored through band-pass filters. The detector consists of a Phillips XP2254/B (red-sensitive version of XP2020) PMT in a thermoelectrically cooled housing. The PMT was operated at −2 kV using an EG&G Ortec 556 power supply. The detector electronics from EG&G Ortec include two 9307 discriminators, a 457 biased time-to-amplitude converter, and a 916A multichannel analyzer. The instrument response function of the setup was ~2 ns (fwhm).

All solutions used in emission measurements were deoxygenated in repeated freeze−pump−thaw cycles. For the incorporation of a sample into PMMA matrix, to a toluene solution of the sample was added PMMA to form a highly viscous polymer blend, followed by wet-casting on a glass slide to obtain a PMMA film embedded with the sample.

Results and Discussion

Characterization. The functionalized carbon nanotube samples $\mathbf{I_{Py}}$-SWNT, $\mathbf{I_{Py}}$-MWNT, and $\mathbf{I_{Py}}'$-SWNT are all soluble in common organic solvents such as chloroform, THF, and toluene, which makes it possible to characterize the materials by using both solution-phase and solid-state techniques.

The ^{1}H NMR spectra of these functionalized carbon nanotube samples in solution all exhibit significantly broader peaks of generally similar chemical shifts to those of $\mathbf{I_{Py}}$ and $\mathbf{I_{Py}}'$, as reported in the Experimental Section. The NMR signal broadening is consistent with the attachment of the pyrene-containing dendra to carbon nanotubes, which are high molecular weight and low mobility species.[21,22] The presence of ester linkages between the dendra and carbon nanotubes is supported by the FT-IR results.[23] For the functionalized carbon nanotube samples in KBr matrix, the FT-IR spectra exhibit ester C═O peaks at 1735 cm^{-1} for $\mathbf{I_{Py}}$-SWNT, 1739 cm^{-1} for $\mathbf{I_{Py}}$-MWNT, and 1736 cm^{-1} for $\mathbf{I_{Py}}'$-SWNT (Figure 1).

The carbon nanotubes are well-dispersed in these soluble samples according to TEM results. For the functionalized MWNTs imaged at a lower resolution, only the nanotubes are visualized (Figure 2) because of their high contrast to the functionalities. At a higher resolution, however, soft materials on the nanotube surface can be observed (Figure 2). These soft materials, also found in the TEM imaging of the functionalized SWNTs,[16,24] may be attributed to the attached $\mathbf{I_{Py}}$ and $\mathbf{I_{Py}}'$ species. The removal of these functionalities from the carbon nanotubes could be achieved via thermal defunctionalization (see below).[21]

As in other well-dispersed functionalized carbon nanotubes, the Raman spectra of the $\mathbf{I_{Py}}$-SWNT, $\mathbf{I_{Py}}$-MWNT, and $\mathbf{I_{Py}}'$-SWNT samples are all overwhelmed by contributions from the strong nanotube defect luminescence.[21,25,26] However, the luminescence interference could be eliminated by measuring

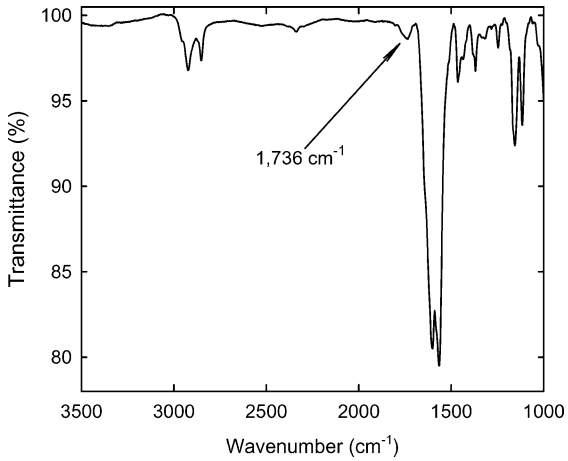

Figure 1. The FT-IR spectrum of $\mathbf{I_{Py}}'$-SWNT in a KBr pellet at room temperature.

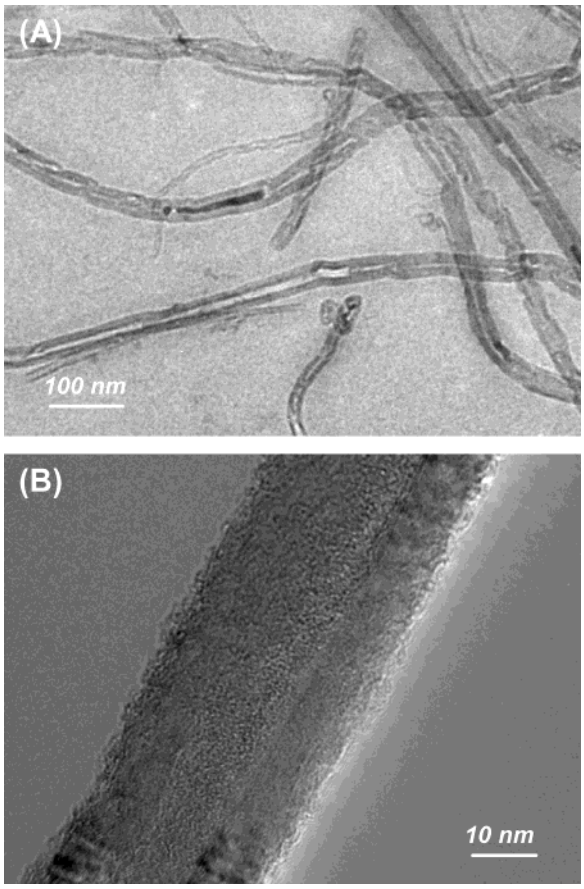

Figure 2. TEM images of the $\mathbf{I_{Py}}$-MWNT sample.

the thermally defunctionalized samples, for which the functionalities on the nanotube surface were removed in slow TGA scans.[21,26] The Raman spectra of the thermally defunctionalized samples exhibit features characteristic of carbon nanotubes.[16]

The TGA measurements were also used to estimate the nanotube contents in the soluble samples, because the functional groups $\mathbf{I_{Py}}$ and $\mathbf{I_{Py}}'$ could be completely removed from the nanotube surface by scanning the temperature to 800 °C in an inert atmosphere. The nanotube contents thus determined for the samples used in this study are on the order of 30% (wt/wt) for $\mathbf{I_{Py}}$-SWNT, 29% (wt/wt) for $\mathbf{I_{Py}}$-MWNT, and 15% (wt/wt) for $\mathbf{I_{Py}}'$-SWNT.

Photophysical Properties. UV/vis absorption spectra of the functionalized carbon nanotubes in room-temperature toluene

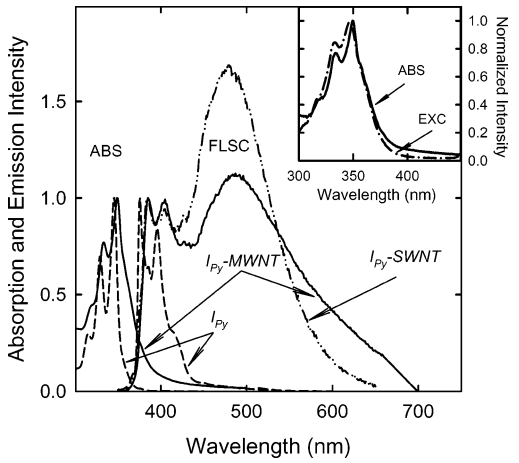

Figure 3. Absorption (ABS) and fluorescence (FLSC, excitation wavelength 337 nm) spectra of $\mathbf{I_{Py}}$ and $\mathbf{I_{Py}}$-MWNT in room-temperature toluene solution, along with the fluorescence spectrum of $\mathbf{I_{Py}}$-SWNT. Shown in the inset is a comparison of the absorption and the fluorescence excitation (EXC, emission wavelength 490 nm) spectra.

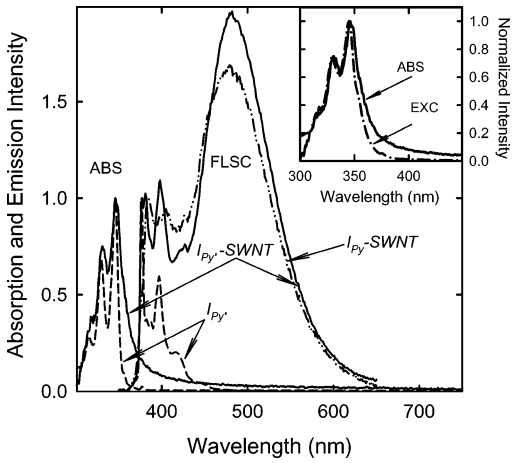

Figure 4. Absorption (ABS) and fluorescence (FLSC, excitation wavelength 337 nm) spectra of $\mathbf{I_{Py}}'$ and $\mathbf{I_{Py}}'$-SWNT in room-temperature toluene solution, along with the fluorescence spectrum of $\mathbf{I_{Py}}$-SWNT. Shown in the inset is a comparison of the absorption and the fluorescence excitation (EXC, emission wavelength 490 nm) spectra.

solution are compared in Figures 3 and 4 with those of $\mathbf{I_{Py}}$ and $\mathbf{I_{Py}}'$. The spectra of $\mathbf{I_{Py}}$ and $\mathbf{I_{Py}}'$ are characterized by the typical derivatized pyrene absorption bands in the 300−400 nm wavelength region. Upon the nanotube attachment, these absorption bands are somewhat red-shifted and also become broader, which may be attributed to effects of the heterogeneous environment associated with a distribution of functionalization sites on the nanotube surface. The spectral changes are consistent with $\mathbf{I_{Py}}$ and $\mathbf{I_{Py}}'$ being linked to the nanotube, against the possibility for simple dendron−nanotube mixtures. The pyrene absorption bands in $\mathbf{I_{Py}}'$-SWNT are structurally better resolved than those in $\mathbf{I_{Py}}$-SWNT and $\mathbf{I_{Py}}$-MWNT (Figures 3 and 4), reflecting the effect of a longer tether and thus more flexible pyrene moieties in $\mathbf{I_{Py}}'$-SWNT. The carbon nanotube absorption is relatively much weaker than the pyrene absorption in the same wavelength region, so its minor contributions can be observed only at longer wavelengths (>400 nm).

Fluorescence spectra of the samples in room-temperature toluene solution with excitation into the pyrene bands are also compared with those of $\mathbf{I_{Py}}$ (Figure 3) and $\mathbf{I_{Py}}'$ (Figure 4). Obviously, both excitation and emission are dominated by the pyrene moieties. The fluorescence spectra of $\mathbf{I_{Py}}$ and $\mathbf{I_{Py}}'$ before

TABLE 1: Observed Fluorescence Quantum Yields[a]

compound	total yield
$\mathbf{I_{Py}}$	0.35
$\mathbf{I_{Py}}'$	0.63
$\mathbf{I_{Py}}$-SWNT	0.07
$\mathbf{I_{Py}}$-MWNT	0.03
$\mathbf{I_{Py}}'$-SWNT	0.27

[a] In toluene solution at 337 nm excitation.

and after the nanotube functionalization are very different. As reported previously for $\mathbf{I_{Py}}$-SWNT,[16] $\mathbf{I_{Py}}$-MWNT and $\mathbf{I_{Py}}'$-SWNT also exhibit significant emission contributions from the pyrene excimer. The assignment of the broad emission band centered at ~490 nm to the pyrene excimer rather than the excitation of pre-associated ground-state pyrene species is supported by results from the fluorescence excitation measurements. As compared in Figures 3 and 4 (insets), the fluorescence excitation spectra obtained by monitoring at 490 nm agree well with the corresponding absorption spectra, except for the longer wavelength region. The difference in that region beyond the pyrene absorption bands is due to the fact that the nanotube absorption does not contribute to the pyrene excimer emission. For all three samples, the excimer emission is independent of the solution concentration, confirming that the excimer formation is "intramolecular" in nature from neighboring pyrene species on the same nanotube.[16]

Fluorescence quantum yields of the $\mathbf{I_{Py}}$-SWNT, $\mathbf{I_{Py}}$-MWNT, and $\mathbf{I_{Py}}'$-SWNT samples in degassed room-temperature toluene solution were determined with excitation into the pyrene absorption bands (337 nm). Here the yields are for total emissions, including both monomer and excimer contributions. As compared in Table 1, the pyrene moieties are much less fluorescent in the functionalized carbon nanotube samples than in $\mathbf{I_{Py}}$ and $\mathbf{I_{Py}}'$. The decrease in fluorescence quantum yield is more pronounced for $\mathbf{I_{Py}}$ before and after the attachment to either SWNT or MWNT (Table 1).

Similar experimental conditions were used in the measurement of fluorescence decays. The fluorescence emissions of $\mathbf{I_{Py}}$ and $\mathbf{I_{Py}}'$ are both long-lived (Figure 5), with single-exponential decay lifetimes of 150 ns and 170 ns, respectively. These lifetime values are comparable to those of other pyrene derivatives. Upon the nanotube attachment, the fluorescence decays with the same excitation wavelength (337 nm) and also the same monitoring wavelength (390 nm) become very different. The fluorescence emissions are overall much shorter-lived in comparison with those of $\mathbf{I_{Py}}$ and $\mathbf{I_{Py}}'$, and the decays all become multiexponential (Figure 5). The excimer emissions (monitored at 490 nm) are also relatively short-lived, with similarly multiexponential decays (Figure 5). The faster decays of both pyrene monomer and excimer emissions are consistent with the lower overall fluorescence quantum yields of the pyrene moieties upon the attachment of $\mathbf{I_{Py}}$ and $\mathbf{I_{Py}}'$ to carbon nanotubes (Table 1).

The excited-state processes in the $\mathbf{I_{Py}}$- and $\mathbf{I_{Py}}'$-functionalized carbon nanotubes are likely complicated, as in other macromolecules containing multiple pyrene species.[27,28] However, qualitatively the absorption and emission results may be explained in terms of a simple scheme shown in Figure 6. Upon the excitation into the pyrene absorption bands, the pyrene monomer excited state is quenched by a neighboring pyrene to form the pyrene excimer. There is another quenching process in which the pyrene monomer excited state undergoes energy transfer to the tethered nanotube.[16] A similar excited-state energy transfer process in the analogous pyrene−fullerene macromolecules has already been reported in the literature.[29] These two

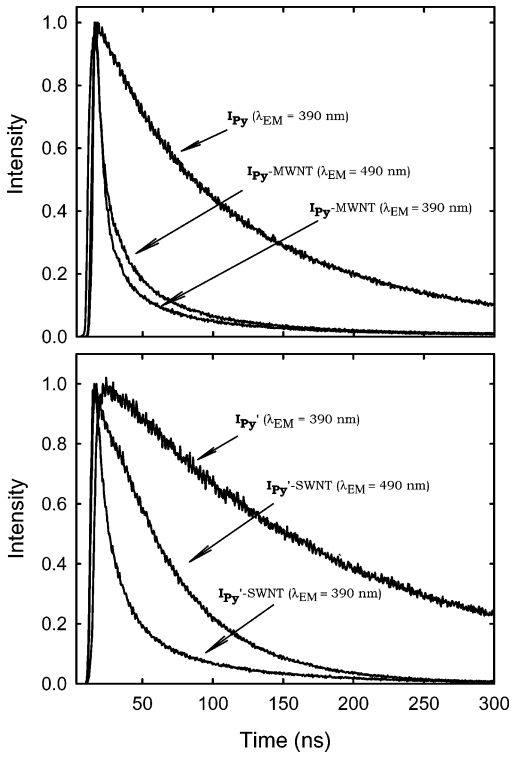

Figure 5. Fluorescence decays (337 nm excitation) in room-temperature toluene solution.

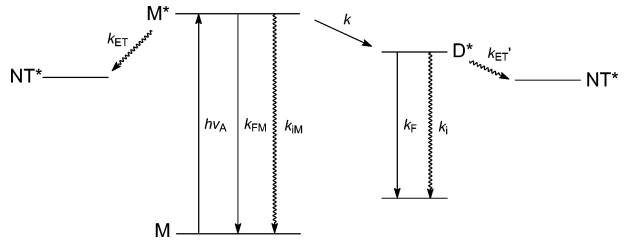

Figure 6. A simplified scheme for the excited-state processes in the $\mathbf{I_{Py}}$- and $\mathbf{I_{Py}}'$-functionalized carbon nanotube samples, where M and D denote pyrene monomer and excimer, respectively, and NT represents the tethered carbon nanotube. The excited-state energy transfer rate constants k_{ET} and k_{ET}' may or may not be the same.

competing quenching processes are responsible for the observed lower quantum yield and faster decay of the pyrene monomer emission in the functionalized carbon nanotube samples. The pyrene excimer emission appears substantial only because it is in reference to the weak pyrene monomer emission (relative to those in the free $\mathbf{I_{Py}}$ and $\mathbf{I_{Py}}'$). The total emission yields are in fact very low (Table 1). Thus, the excited-state energy transfer could still be the dominating process in the quenching of the pyrene monomer excited state, as suggested by the results of $\mathbf{I_{Py}}$-SWNT and $\mathbf{I_{Py}}$-MWNT in the solid state (see below).[16] For the pyrene excimer, there may be similar excited-state energy transfer to the tethered nanotube, contributing to the low overall emission quantum yields. Because the functionalization sites on the nanotube surface are expected to be inhomogeneously distributed, it should not be a surprise for the observed decays to be multiexponential. In addition, the more pronounced decrease of fluorescence quantum yield in $\mathbf{I_{Py}}$ than in $\mathbf{I_{Py}}'$ upon their attachment to carbon nanotubes (Table 1) seems to suggest that the tether length plays a role in the excited-state energy transfer, with the shorter tether being more favorable to the energy transfer.

In a comparison of the three samples, the relative intensities of the pyrene excimer emission are higher in $\mathbf{I_{Py}}$-SWNT than

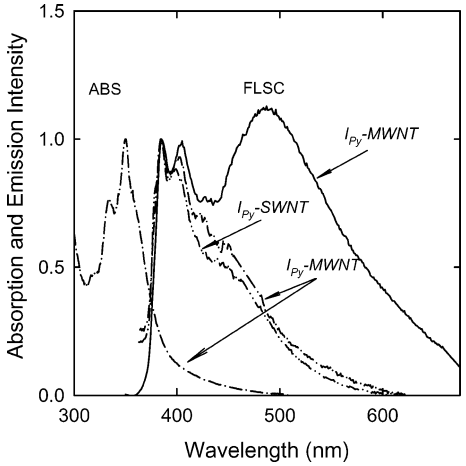

Figure 7. Absorption and fluorescence spectra of $\mathbf{I_{Py}}$-MWNT in the PMMA film at room temperature. The fluorescence spectra of the same sample in room-temperature toluene solution (—) and $\mathbf{I_{Py}}$-SWNT in the PMMA film (—••—) are also shown for comparison.

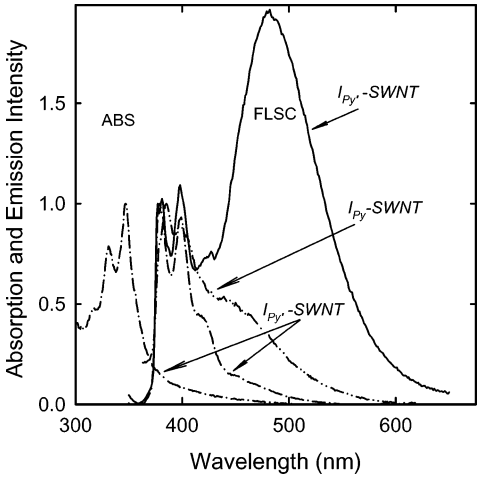

Figure 8. Absorption and fluorescence spectra of $\mathbf{I_{Py}}'$-SWNT in the PMMA film at room temperature. The fluorescence spectra of the same sample in room-temperature toluene solution (—) and $\mathbf{I_{Py}}$-SWNT in the PMMA film (—••—) are also shown for comparison.

in $\mathbf{I_{Py}}$-MWNT (Figure 3). This might be related to the difference in structural flexibility between SWNT and MWNT. The more flexible structure of SWNT may benefit the "intramolecular" pyrene excimer formation, which is primarily dynamic in nature. The pyrene moieties in $\mathbf{I_{Py}}'$-SWNT are in an even more flexible environment because of the extended tether, resulting in the highest relative intensities of the pyrene excimer emission. The more structured spectrum of pyrene monomer emission in $\mathbf{I_{Py}}'$-SWNT is consistent with the expected more flexible environment for the pyrene moieties.

The pyrene excimer formation being dynamic in nature is supported by the spectroscopic results of the $\mathbf{I_{Py}}$- and $\mathbf{I_{Py}}'$-functionalized carbon nanotubes in solid-state polymer matrix. Shown in Figures 7 and 8 are the absorption and fluorescence spectra of the three samples in PMMA films at room temperature. While the absorption spectra are largely similar to those in solution, the fluorescence spectra become very different, without the significant pyrene excimer emission bands observed in solution. Generally speaking, the lack of mobility for the pyrene moieties in the polymer matrix hinders the dynamic process of pyrene excimer formation. However, there is a significant difference between the fluorescence spectra of the nanotube-tethered $\mathbf{I_{Py}}$ (Figure 7) and $\mathbf{I_{Py}}'$ (Figure 8) in PMMA films. The difference is reproducible and striking, but the mechanistic implication is unclear. Further investigations are required for an understanding of the different fluorescence spectra.

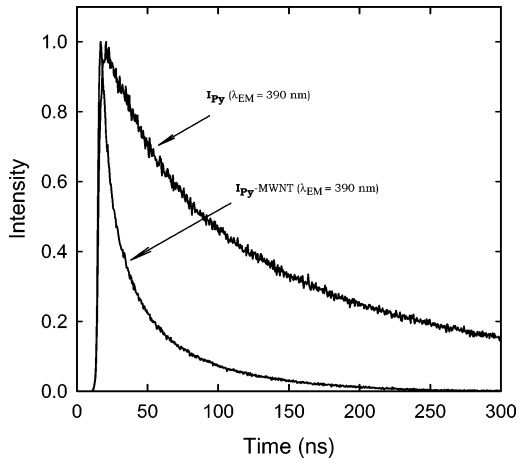

Figure 9. Fluorescence decays (337 nm excitation) in the PMMA film at room temperature.

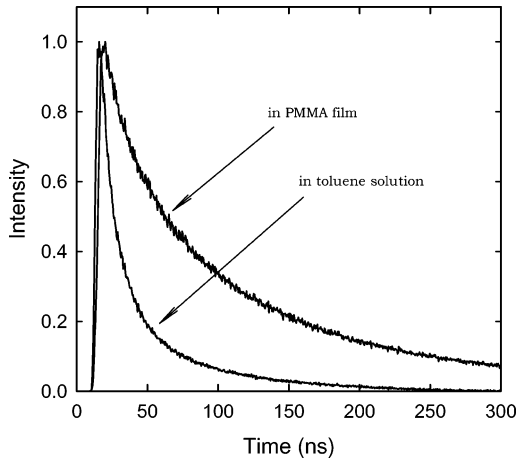

Figure 10. Fluorescence decays (excited at 337 nm and monitored at 390 nm) of $\mathbf{I_{Py}}'$-SWNT at room temperature.

Fluorescence decays of the $\mathbf{I_{Py}}$- and $\mathbf{I_{Py}}'$-functionalized carbon nanotubes in the polymer matrix were measured at 337 nm excitation. For the comparison between the decays of $\mathbf{I_{Py}}$ and $\mathbf{I_{Py}}$-MWNT, as an example, the results in the polymer film and in solution are similar (Figure 9). The pyrene emission in $\mathbf{I_{Py}}$-MWNT is still much shorter-lived than that in $\mathbf{I_{Py}}$ in the solid-state matrix, despite the absence of the quenching associated with the excimer formation. Similar results were obtained from the same comparison between $\mathbf{I_{Py}}$-SWNT and $\mathbf{I_{Py}}$.[16] Thus, it seems that the energy transfer is indeed the dominating deactivation pathway of the pyrene excited state in the $\mathbf{I_{Py}}$-functionalized carbon nanotube samples. Unlike the excimer formation, the excited-state energy transfer is insensitive to the change in medium from solution to solid-state polymer film.

In $\mathbf{I_{Py}}'$-SWNT, the quenching of the excited pyrene by neighboring pyrene moieties is probably more significant in the competition with the process of energy transfer to the tethered nanotube (Figure 6). As shown in Figure 10, the pyrene fluorescence is in general longer-lived for $\mathbf{I_{Py}}'$-SWNT in the polymer film than in toluene solution. The slower decay, though still multiexponential, reflects the suppression of excimer formation in the solid-state polymer matrix. In fact, the pyrene moieties in $\mathbf{I_{Py}}'$-SWNT are expected to be structurally more flexible because of the longer tether. The more efficient excimer

formation in $\mathbf{I_{Py}}'$-SWNT, as suggested by the results discussed above, is consistent with such an expectation.

The decoration of carbon nanotubes with tethered pyrene species may serve several purposes. First, the excited pyrene moieties before the nanotube attachment are long-lived, thus ideal probes for interactions with and energy transfer to the nanotube. The excited-state energy transfer is apparently dependent on the tether length, which offers opportunities to the manipulation and control of pyrene−nanotube interactions. Second, the formation of excimer between the tethered pyrene moieties may be used in the study of local environment on the carbon nanotube surface. Since the functionalization is based on the surface defects, the "intramolecular" and inter-tether excimer may be targeted in further investigations for information on the population and location of defect sites on the carbon nanotube. Third, the functionalized carbon nanotubes with covalently linked pyrene species may be studied as models for a new class of photoactive carbon nanomaterials. Potential applications of carbon nanotubes-based photoactive materials have been widely discussed in the literature. Finally, pyrene has been associated with carbon nanotubes in various configurations. The pyrene−nanotube materials reported here are structurally defined. These systems of less ambiguous configurations are valuable to the effort toward a fundamental understanding of pyrene−nanotube interactions and also chromophore−nanotube interactions in general.

Acknowledgment. We thank Prof. A. M. Rao for supplying the carbon nanotube samples and B. Zhou for experimental assistance. Y.-P.S. acknowledges financial support from NSF, NASA, the South Carolina Space Grant Consortium, and the Center for Advanced Engineering Fibers and Films (NSF-ERC at Clemson University). C.E.B. thanks AFOSR and Dr. J. Tishkoff for financial support. We also acknowledge the sponsorship by the Assistant Secretary for Energy Efficiency and Renewable Energy, Office of Transportation Technologies, as part of the HTML User Program, Oak Ridge National Laboratory, managed by UT-Battelle, LLC. for DOE (DE-AC05-00OR22725).

Supporting Information Available: NMR data for 1-pyrenebutanbromide (**1**), methyl 3-hydroxy-5-hexadecoxy benzoate (**2**), and methyl 3-hexadecoxy-5-pyrenebutanoxyl benzonate (**3**). This material is available free of charge via the Internet at http://pubs.acs.org.

References and Notes

(1) Ouyang, M.; Huang, J.-L.; Lieber, C. M. *Acc. Chem. Res.* **2002**, *35*, 1018.

(2) Avouris, P. *Acc. Chem. Res.* **2002**, *35*, 1026.

(3) Dai, H. *Acc. Chem. Res.* **2002**, *35*, 1035.

(4) Davis, J. J.; Coleman, K. S.; Azamian, B. R.; Bagshaw, C. B.; Green, M. L. H. *Chem. Eur. J.* **2003**, *9*, 3732.

(5) Lin, Y.; Taylor, S.; Li, H.; Fernando, K. A. S.; Qu, L.; Wang, W.; Gu, L.; Zhou, B.; Sun, Y.-P. *J. Mater. Chem.* **2004**, *14*, 527.

(6) (a) Star, A.; Stoddart, J. F.; Steuerman, D. W.; Diehl, M. R.; Boukai, A.; Wong, E. W.; Yang, X.; Chung, S.-W.; Choi, H.; Heath, J. R. *Angew. Chem., Int. Ed.* **2001**, *40*, 1721. (b) Steuerman, D. W.; Star, A.; Narizzano, R.; Choi, H.; Ries, R. S.; Nicolini, C.; Stoddart, J. F.; Heath, J. R. *J. Phys. Chem. B* **2002**, *106*, 3124. (c) Star, A.; Liu, Y.; Grant, K.; Ridvan, L.; Stoddart, J. F.; Steuerman, D. W.; Diehl, M. R.; Boukai, A.; Heath, J. R. *Macromolecules* **2003**, *36*, 553.

(7) Guldi, D. M.; Marcaccio, M.; Paolucci, D.; Paolucci, F.; Tagmatarchis, N.; Tasis, D.; Vazquez, E.; Prato, M. *Angew. Chem., Int. Ed.* **2003**, *42*, 4206.

(8) Zhu, W.; Minami, N.; Kazaoui, S.; Kim, Y. *J. Mater. Chem.* **2003**, *13*, 2196.

(9) Alvaro, M.; Atienzar, P.; Bourdelande, J. L.; Garcia, H. *Chem. Phys. Lett.* **2004**, *384*, 119.

(10) Li, H.; Zhou, B.; Lin, Y.; Gu, L.; Wang, W.; Fernando, K. A. S.; Kumar, S.; Allard, L. F.; Sun, Y.-P. *J. Am. Chem. Soc.* **2004**, *126*, 1014.

(11) Nakashima, N.; Tomonari, Y.; Murakami, H. *Chem. Lett.* **2002**, 638.

(12) Liu, L.; Wang, T.; Li, J.; Guo, Z.-X.; Dai, L.; Zhang, D.; Zhu, D. *Chem. Phys. Lett.* **2003**, *367*, 747.

(13) Murakami, H.; Nomura, T.; Nakashima, N. *Chem. Phys. Lett.* **2003**, *378*, 481.

(14) Zhang, J.; Lee, J.-K.; Wu, Y.; Murray, R. W. *Nano Lett.* **2003**, *3*, 403.

(15) Georgakilas, V.; Kordatos, K.; Prato, M.; Guldi, D. M.; Holzinger, M.; Hirsch, A. *J. Am. Chem. Soc.* **2002**, *124*, 760.

(16) Qu, L.; Martin, R. B.; Huang, W.; Fu, K.; Zweifel, D.; Lin, Y.; Sun, Y.-P.; Bunker, C. E.; Harruff, B. A.; Gord, J. R.; Allard, L. F. *J. Chem. Phys.* **2002**, *117*, 8089.

(17) Journet, C.; Maser, W. K.; Bernier, P.; Loiseau, A.; de la Chapelle, M. L.; Lefrant, S.; Deniard, P.; Lee, R.; Fischer, J. E. *Nature* **1997**, *388*, 756.

(18) (a) Andrews, R.; Jacques, D.; Rao, A. M.; Derbyshire, F.; Qian, D.; Fan, X.; Dickey, E. C.; Chen, J. *Chem. Phys. Lett.* **1999**, *303*, 467. (b) Rao, A. M.; Jacques, D.; Haddon, R. C.; Zhu, W.; Bower, C.; Jin, S. *Appl. Phys. Lett.* **2000**, *76*, 3813.

(19) Hu, H.; Zhao, B.; Itkis, M. E.; Haddon, R. C. *J. Phys. Chem. B* **2003**, *107*, 13838.

(20) The NMR data are provided in Supporting Information.

(21) Sun, Y.-P.; Fu, K.; Lin, Y.; Huang, W. *Acc. Chem. Res.* **2002**, *35*, 1096.

(22) Sun, Y. P.; Huang, W.; Lin, Y.; Fu, K.; Kitaygorodskiy, A.; Riddle, L. A.; Yu, Y. J.; Carroll, D. L. *Chem. Mater.* **2001**, *13*, 2864.

(23) (a) Chen, J.; Hamon, M. A.; Hu, H.; Chen, Y.; Rao, A. M.; Eklund, P. C.; Haddon, R. C. *Science* **1998**, *282*, 95. (b) Hamon, M. A.; Chen, J.; Hu, H.; Chen, Y.; Rao, A. M.; Eklund, P. C.; Haddon, R. C. *Adv. Mater.* **1999**, *11*, 834. (c) Hamon, M. A.; Hu, H.; Bhowmik, P.; Itkis, M. E.; Haddon, R. C. *Appl. Phys. A* **2002**, *74*, 333.

(24) Lin, Y.; Hill, D. E.; Bentley, J.; Allard, L. F.; Sun, Y.-P. *J. Phys. Chem. B* **2003**, *107*, 10453.

(25) (a) Riggs, J. E.; Guo, Z.; Carroll, D. L.; Sun, Y.-P. *J. Am. Chem. Soc.* **2000**, *122*, 5879. (b) Sun, Y.-P.; Zhou, B.; Henbest, K.; Fu, K.; Huang, W.; Lin, Y.; Taylor, S.; Carroll, D. L. *Chem. Phys. Lett.* **2002**, *351*, 349.

(26) Huang, W.; Fernando, S.; Lin, Y.; Zhou, B.; Allard, L. F.; Sun, Y.-P. *Langmuir* **2003**, *19*, 7084.

(27) (a) Zachariasse, K. A.; Duveneck, G.; Busse, R. *J. Am. Chem. Soc.* **1984**, *106*, 1045. (b) Zachariasse, K. A.; Duveneck, G.; Kunhle, W. *Chem. Phys. Lett.* **1985**, *113*, 337. (c) Zachariasse, K. A.; Striker, G. *Chem. Phys. Lett.* **1988**, *145*, 251. (d) Zachariasse, K. A.; Kuhnle, W.; Leinhos, U.; Reynders, P.; Striker, G. *J. Phys. Chem.* **1991**, *95*, 5476. (e) Zachariasse, K. A.; Macanita, A. L.; Kuhnle, W. *J. Phys. Chem. B* **1999**, *103*, 9356.

(28) (a) Webber, S. E. *Chem. Rev.* **1990**, *90*, 1469. (b) Stramel, R. D.; Nguyen, C.; Webber, S. E.; Rodgers, M. A. J. *J. Phys. Chem.* **1988**, *92*, 2934.

(29) (a) Martin, R. B.; Fu, K.; Sun, Y.-P. *Chem. Phys. Lett.* **2003**, *375*, 619. (b) Martin, R. B.; Fu, K.; Li, H.; Cole, D.; Sun, Y.-P. *Chem. Commun.* **2003**, 2368.